Polypyrrole-coated Graphite Fluorides with High Energy and High Power Densities for Li/CF$_x$ battery

Ling Zhu, Lei Li, Jie Zhou, Yong Pan[*] *, Weixin Lei*[*] *, Zengsheng Ma*

Hunan Provincial Key Laboratory of Thin Film Materials and Devices and School of Materials Science and Engineering, Xiangtan University, Hunan 411105 China
[*]E-mail: ypan@xtu.edu.cn, wxlei@xtu.edu.cn

Polypyrrole (PPy) coated graphite fluorides (CF$_x$) composites have been prepared via in situ chemical oxidative polymerization. The influence of coating thickness on the electrochemical performances of PPy-coated CF$_x$ (CF$_x$@PPy) cathodes has been investigated. The results show that the rate capability of CF$_x$@PPy cathodes are improved compared with that of pristine CF$_x$ cathode. The PPy coating serves as the path for charges transfer from the surface of CF$_x$ to the reaction interface. The conductivity of CF$_x$@PPy increases with the growing PPy coating, however, too thick PPy coating may inhibit the lithium ions transfer and even pull down the discharge capacity. Finally, the CF$_x$@PPy composite with a PPy coating thickness of 80 nm exhibits a superior rate capability and a maximum delivered power density up to 7091 W kg^{-1} at 6 C.

1. INTRODUCTION

Lithium batteries are commonly used for many applications such as cameras, electrical lock, electronic counter, electronic measurement equipment, emergency power source, memory back-up, military and implantable medical devices [1-3]. These applications require power sources with high energy densities, good reliability, safety and long life. Li/graphite fluoride (CF$_x$) batteries have been paid attention for the high specific capacity, flat discharge potential, low self-discharge and wide operating temperature (−40 to 170 ℃) [4-7]. Li/CF$_x$ cell can be used in advanced devices which need long time sustained discharges, such as medical implants, army applications and aero-equipments, because its high theoretical specific capacity, up to 865 mAh g^{-1}[8].

Due to the strong covalent C-F bond, the electrical conductivity of CF$_x$ is very low [9]. Therefore, the CF$_x$ cathode shows a significant polarization and a lower discharge voltage (around 2.4

V) than the open circuit voltage (3.2–3.5 V) used in Li/CF$_x$ cells [10], which inhibits the application of CF$_x$ in high power devices. The sub-fluorinated graphite [11-13] and low temperature CF$_x$ [14-17] can improve the rate capability of CF$_x$ for the presences of unfluorinated domains and promot electrons transfer in CF$_x$, however, the specific capacities of CF$_x$ decreases due to the low fluorine contents. Also, the thermal treatment of CF$_x$ can enhance the electrochemical performances due to the carbon formation by the partial decomposition of CF$_x$ [18-20]. Hybrid cathodes combining CF$_x$ with other cathode materials, such as MnO_2 or $Ag_2V_4O_{11}$, are considered to improve the rate capability of CF$_x$ [8, 21-22].

Furthermore, it is possible to prepare the CF$_x$@coatings cathodes as an effective approache to improve electrochemical performances of CF$_x$ cathodes [23-25]. For example, Zhang et al. [25] prepared the carbon-coated CF$_x$ by heat treating the mixture of CF$_x$ and polyvinylidence difluoride (PVDF). The coated CF$_x$ could discharge steadily at 2 C with a specific capacity of 370 mAh g^{-1}. The carbon coating improved the particle connection and favored the electron pathway through the electrode and thus increased the power density. Zhu et al. [26] prepared the sperical carbon-coated CF$_x$ by microencapsulation and concentrated sulfuric acid carbonization. The maximun discharge rate is improved from 0.5 C by CF$_x$ to 5 C by the carbon coated CF$_x$. The high power density of the carbon coated CF$_x$ was attributed to the enhanced combination of active material and conductive agent, good electronic conductivity provided by the carbon coating and the porous surface which could store much electrolyte and allows more channels for the Li$^+$ ion transferring. Groult et al. [27] improved the electrochemical features of graphite fluoride by electrodepositing a polypyrrole (PPy) layer on the CF$_x$ cathode and obtained a maximum power density of 5235 W kg^{-1} (4 C-rate) with PPy–CF$_{0.80}$.

As a soft conducting polymer, PPy coating has been investigated on many electrode materials to enhance their electrochemical performances. Zhi-jia Zhang et al. [28] studied the polypyrrole-coated α-LiFeO$_2$ nanocomposite for lithium-ion batteries. It was found that the conductive PPy served as both a conducting matrix and a protective coating to enhance the capacity retention and rate capability. Jingchao Cao et al. [29] investigated the polypyrrole-coated LiCoO$_2$ nanocomposite for lithium-ion batteries. The results showed that the charge-transfer resistance decreased and the reversible capacity retention increased after being coated with PPy. The PPy film acted as a capsule shell, which could protect the core (LiCoO$_2$) from corrosion causing by the HF attacking and greatly reduce the dissolution of Co into electrolyte.

In this study, the CF$_x$ particles have been coated by PPy. The PPy coating which acts as an electronic conductivity layer is synthesized via in situ chemical oxidative polymerization. The effect of coating thickness on the structure and electrochemical performances of CF$_x$@PPy has been investigated. With the exterior electronic pathway provided by the PPy, the CF$_x$@PPy cathodes achieve a superior rate capability than that of the pristine CF$_x$.

2. EXPERIMENTAL

2.1. Preparation of CF$_x$@PPy

The CF$_x$@PPy composites were synthesized by in situ chemical oxidative polymerization at the freezing temperature in a mixed solution. The CF$_x$ (1 g) powders (Shanghai CarFluor Chemicals Co.,

Ltd) was placed into deionized water (10 mL) with the OP-10 emulsifier (Tianjin Chemical Reagent Company). The CF_x powders could be homogeneously dispersed by mechanical stirring for 30 min and magnetic stirring for 6 h. Certain amount of pyrrole monomers (Sinopharm Chemical Reagent Co., Ltd), which had been purified by distillation beforehand, were added into the dilute hydrochloric acid solution (2 mol L^{-1}, 5 mL). The CF_x solutions and the pyrrole monomers solutions were put into the three-necked flask together and stirred vigorously for 10 min. Then, a hydrochloric acid solution (5 mL) containing $(NH_4)_2S_2O_8$ (Kermel Reagent) was added dropwise into the above mixture and reacted for 12 h at 0 ℃. The $(NH_4)_2S_2O_8$ acted as an oxidant and the weight ratio of $(NH_4)_2S_2O_8$ to pyrrole monomers was 4:1. The reaction products were filtered and washed repeatedly with deionized water and ethanol in order to remove the hydrochloric acid and the unreacted pyrrole monomers, respectively, until the washing solution reached neutral pH and became transparent. Finally, the products were dried in a vacuum oven at 60 ℃ for 24 h and the pure CF_x@PPy composites were obtained. Here, the mass ratios of CF_x and pyrrole monomers were chose as 2:1, 8:1 and 16:1, respectively.

2.2. Structural Characterization

X-ray diffraction (XRD) measurements were made using a Rigaku D/Max-2400 X-ray diffractometer with Cu K_α radiation ($\lambda = 0.1542$ nm). The surface morphologies and microstructures of the pristine CF_x and CF_x@PPy composites were characterized by scanning electron microscopy (SEM, Hitachi S-4800) and JEM-2100 transmission electron microscopy (TEM), respectively. The elemental analysis was carried out by the Oxford EDX analysis system.

2.3. Electrochemical measurements

The CF_x and CF_x@PPy composites were used as active cathode materials. The electrodes were composed of active materials (70 *wt.*%), acetylene black (20 *wt.*%) to ensure electronic conductivity and polyvinylidene fluoride (10 *wt.*%) as binder. N-methyl pyrrolidone (NMP) was added to form uniform slurry. The slurry was compressed into a thin piece with coating machine, and then dried in a vacuum oven at 60 ℃ for 12 h. The electrode was cut into disks of 14 mm diameter. The coin-type 2016 cells were assembled in an argon-filled glovebox to avoid contamination by moisture and oxygen. The solution of 1 M $LiPF_6$ in ethylene carbonate (EC): dimethyl carbonate (DMC) (1:1, vol.) was employed as the electrolyte. Lithium metal was used as an anode and a microporous polypropylene film (Celgard 2400) was used as a separator.

All the electrochemical measurements were carried out at room temperature. Galvanostatic discharges were carried out on a Neware battery test station. Electrochemical impedance spectroscopy (EIS) was measured by a CHI660D Electrochemical Workstation (Chenhua, Shanghai, China) in the frequency range from 0.1 Hz to 1000 kHz.

3. RESULTS AND DISCUSSION
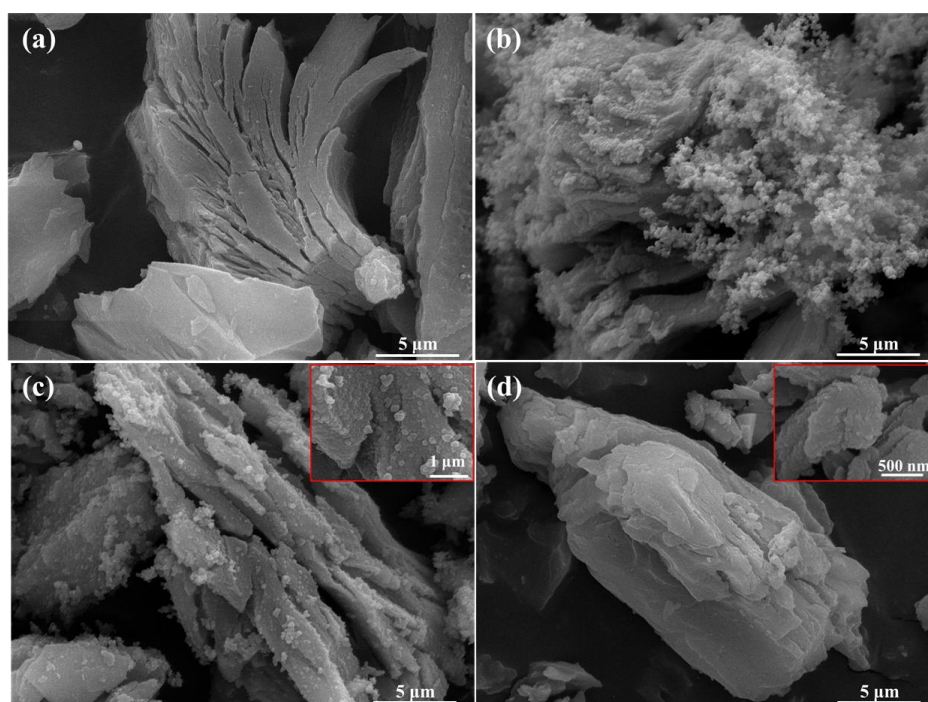
Figure 1. SEM images of (a) pristine CF$_x$, (b) CF$_x$@PPy(2:1), (c) CF$_x$@PPy(8:1), and (d) CF$_x$@PPy(16:1).
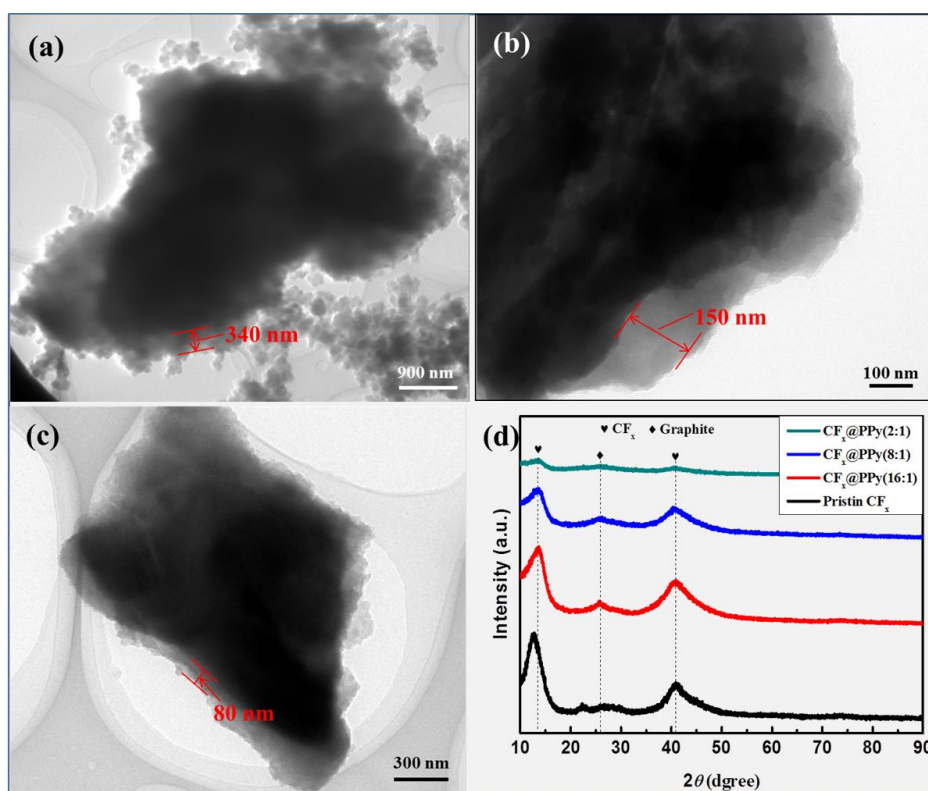
Figure 2. TEM images of (a) CF$_x$@PPy(2:1), (b) CF$_x$@PPy(8:1), (c) CF$_x$@PPy(16:1); and (d) XRD patterns of pristine CF$_x$ and CF$_x$@PPy composites.
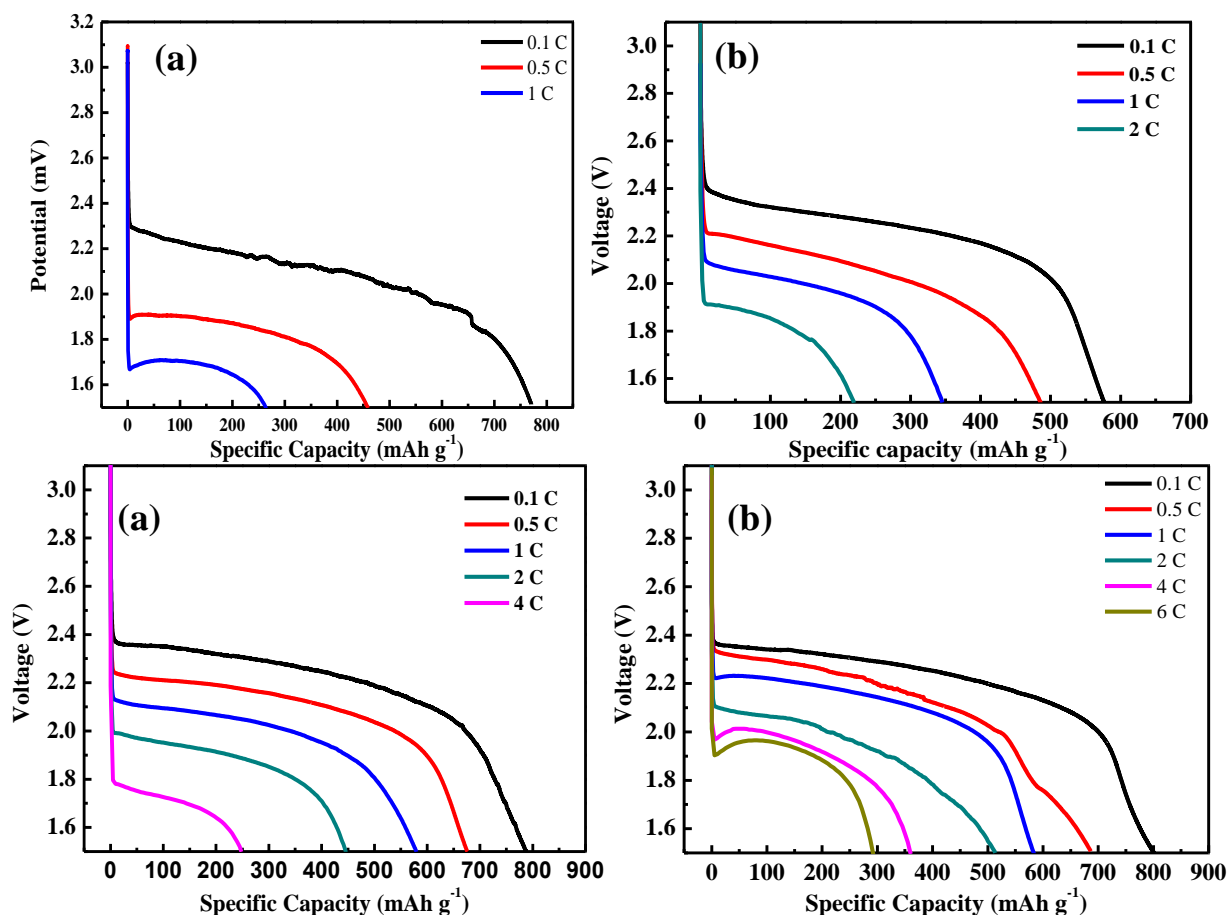
Figure 3. Galvanostatic discharge curves of (a) pristine CF_x, (b) $CF_x@PPy(2:1)$, (c) $CF_x@PPy(8:1)$, and (d) $CF_x@PPy(16:1)$ at different rates.

Fig. 1 shows the SEM images of the pristine CF_x and $CF_x@PPy$ composites. It can be seen that the CF_x has been coated by PPy successfully. The layer-structrual CF_x becomes mellow at the edges and corners after coated process in Fig. 1a. The PPy layer is transparent and very thin uniformly on the surface of $CF_x@PPy(16:1)$, as shown in Fig. 1d. The EDS spectrums (not shown here) of which the nitrogen element has been detected further convince the existence of PPy coating. From the enlarged view of Fig. 1c and Fig. 1d, we can see there are some islands of PPy on the surface of $CF_x@PPy$. The PPy layer also can coat the inner surface of the layer spacing in CF_x perfectly. As the PPy content increasing, the quantity and bulk of PPy islands increase fast. Finally, the dendritic PPy particles come into being (Fig. 1b).

To determine the thicknesses of PPy coating, TEM images of $CF_x@PPy$ composites are presented in Fig. 2. From the images, we can see that the thickness of $CF_x@PPy(2:1)$, $CF_x@PPy(8:1)$ and $CF_x@PPy(16:1)$ are 340 nm, 150 nm and 80 nm, respectively. Some scattered PPy particles exist around the $CF_x@PPy(2:1)$ in Fig. 2a, because the PPy layer of $CF_x@PPy$ is very thick with the increasing pyrrole monomers in the polymerization. We conclude that the PPy coating forms uniformly first, then becomes thicker and finally generate dendritic PPy particles as the PPy content increase.

Fig. 2d shows the XRD patterns of CF_x and $CF_x@PPy$ composites. The broad peaks corresponding to the CF_x phases at around 13.6° and 41.1° (JCPDS 30-0476) and graphite phases at 25.6°(JCPDS 26-1076) are observed on CF_x and $CF_x@PPy$ composites. The presence of graphite phases indicates that the basic layer structure of graphite of pristine CF_x. PPy phase is not observed in this pattern. However, the intensity of broad peaks of $CF_x@PPy$ composites decrease. This may be due to the pyrrole coating on the surface that hinder the signal to be detected.

Fig. 3 presents the galvanostatic discharge curves of the pristine CF_x and $CF_x@PPy$ composites at different current rates. The electrochemical performances are summarized in Table 1.

The pristine CF_x exhibits a poor rate capability and its specific capacity is 773 mAh g^{-1} at 0.1 C and 264 mAh g^{-1} at 1 C. The low discharge rates of CF_x inhibits the application in the fields requiring high power densities. The $CF_x@PPy$ composites exhibit higher rate capability than that of the pristine CF_x due to the existence of PPy coating. The specific capacities of $CF_x@PPy(2:1)$, $CF_x@PPy(8:1)$ and $CF_x@PPy(16:1)$ are 345 mAh g^{-1}, 579 mAh g^{-1}, 583 mAh g^{-1} at 1 C, respectively. It is noted that the rate capability of $CF_x@PPy$ composites shows a significant dependence on the thickness of PPy coating. CF_x coated with 80 nm PPy exhibits the best rate capability at 6 C with a specific capacity of 294 mAh g^{-1}, which shows better electrochemical performances than the former reported [27] PPy coated CF_x. The maximum discharge rate of the former reported PPy coated CF_x is 4 C, associated with a specific capacity of 70 mAh g^{-1}. The differences may crucially depend on the coating level of PPy. PPy can be coated on the inner surface of the layer spacing in CF_x of $CF_x@PPy(16:1)$ that may greatly improve the rate capability.

Table 1. Electrochemical performances of batteries with different cathodes.

Samples	C-rate	Average Potential (V)	Specific Capacity (mAh g^{-1})	Energy density (Wh kg^{-1})	Average Power Density(W kg^{-1})
CF$_x$	0.1 C	2.10	773	1534	174
	0.5 C	1.85	459	865	801
	1 C	1.70	264	460	1468
CF$_x$@PPy(2:1)	0.1 C	2.24	576	1264	183
	0.5 C	2.06	486	980	880
	1 C	1.98	345	670	1544
	2 C	1.84	219	395	3123
CF$_x$@PPy(8:1)	0.1 C	2.25	788	1727	186
	0.5 C	2.14	676	1411	841
	1 C	2.03	579	1145	1683
	2 C	1.9	445	833	2911
	4 C	1.72	248	421	5872
CF$_x$@PPy(16:1)	0.1 C	2.25	801	1754	202
	0. 5 C	2.17	686	1430	875
	1 C	2.15	583	1223	1865
	2 C	1.96	514	985	3385
	4 C	1.94	361	683	6624
	6 C	1.93	294	565	7091
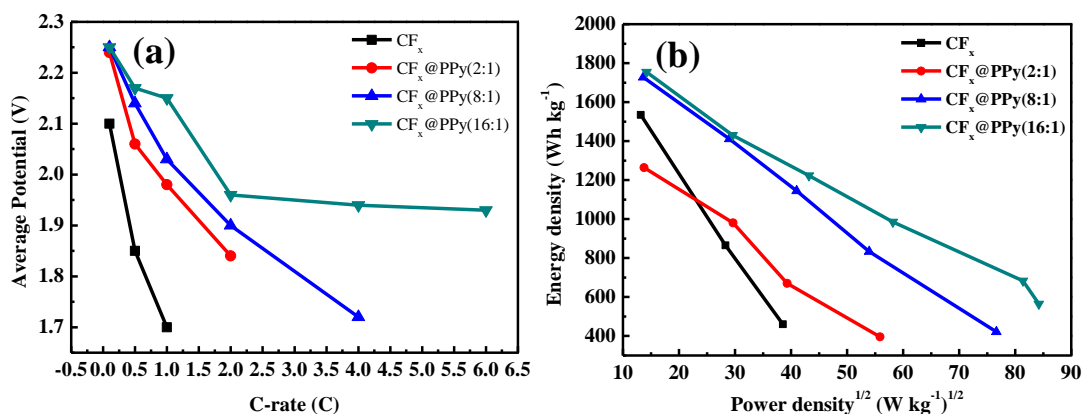
Figure 4. (a) Average potential as a function of discharge rate and (b) the Ragone plot of the pristine CF_x and CF_x@PPy composites.

CF_x coated with 150 nm and 340 nm PPy can only work at 4 C and 2 C with the specific capacities of 248 mAh g^{-1} and 219 mAh g^{-1}, respectively. The CF_x@PPy with thicker PPy coating shows a poorer rate capability, indicating that the discharge process may be blocked by the excessive PPy at high discharge rates.

Fig. 4a shows the average potential of the pristine CF_x and CF_x@PPy composites as a function of discharge rate. It is clear that the average potential of the pristine CF_x decreases rapidly as increasing discharge rate. The downtrend of average potential is relieved by coating PPy layer on CF_x. The thinner the PPy coating, the slower the average potential downtrend. The average potential of CF_x@PPy(16:1) can be hold on 1.93 V at 6 C, while it is only 1.70 V at 1 C for CF_x. Fig. 4b shows the energy densities versus power densities of CF_x@PPy composites. At low discharge rate, less than 1 C, the delivered energy densities of CF_x@PPy(8:1) are close to those of CF_x@PPy(16:1). With increasing the power density, the energy densities of CF_x@PPy(8:1) decrease more rapidly than those of CF_x@PPy(16:1). The CF_x@PPy(16:1) exhibits the best electrochemical performances with the maximum power density of 7091 W kg^{-1} at 6 C and the energy density of 565 Wh kg^{-1}. However, the delivered energy density of CF_x@PPy(2:1) is lower than that of the pristine CF_x at 1 C, which may be contributed to the thick PPy coating owning low specific energy.

Sub-fluorinated graphites [30-31] can improve the rate capability of CF_x because the presence of unfluorinated domains that facilitate electrons transport within CF_x. The fluorinated carbon nanofibres with F:C = 0.76 [31] can get a highest power density of 8057 W kg^{-1} at 6 C. However, the specific capacity of CF_x is decreased due to the lowered fluorine content. The CF_x@PPy can get high rate capability with a very thin film of PPy wich does not influence the specific capacity much. What's more, the commercial CF_x used in CF_x@PPy is much cheaper than the fluorinated carbon nanofibres. The CF_x@PPy is promising to be applied in commercial Li/CF_x cells.

To further reveal the electrochemical mechanism of CF_x@PPy cathodes, the electrochemical impedance spectroscopy (EIS) was presented in Fig. 5.
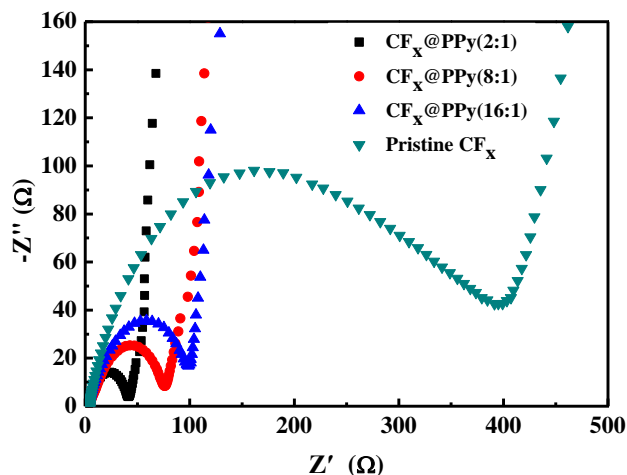
Figure 5. EIS patterns of pristine CF_x and CF_x@PPy composites.

The depressed semicircle in the impedance corresponds to the cell reaction resistance (R_{cr}), which is the synergetic effects of the contact resistance between particles, product shell and charge-transfer of the electrolyte-electrode interface. The R_{cr} of the pristine CF_x about 400 Ω is much higher than that of CF_x@PPy composites. The R_{cr} of CF_x@PPy composites decrease dramatically with the increase of thickness of PPy layer, proving that the conductivity of CF_x@PPy cathodes is improved by the PPy coating. The PPy thin film on the CF_x constructs conductive network, that is beneficial to electrons transfer and Li$^+$ ions diffusion during discharge process. As a result, a high energy and high power density of the CF_x@PPy is abtained.
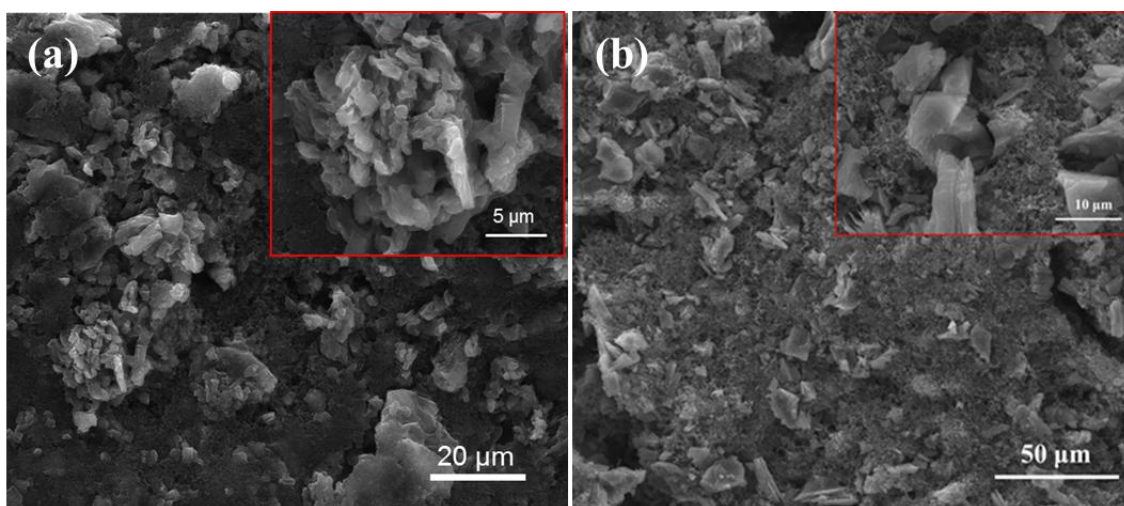
Figure 6. SEM images of discharged cathodes at 0.1 C: (a) CF_x@PPy(16:1) and (b) CF_x.

Both fully discharged (at 0.1 C) pristine CF_x and CF_x@PPy cathodes are tested by SEM (Fig. 6). Due to the low surface energy of CF_x, the combination between CF_x and acetylene black is weak and the cathode (Fig. 6b) presents a loosen structure. In contrast, the CF_x@PPy particles are tightly bonded

with acetylene black, which guarantees the electrons transferring from Al collector to cathode materials (Fig. 6a). It indicates that the adsorptivity of CF_x has been improved by PPy coating. So the CF_x@PPy cathode is much easier to be infiltrated by electrolyte than the pristine CF_x cathode.

4. CONCLUSIONS

PPy-coated CF_x composites with different PPy thickness have been synthesized for lithium primary batteries. The electrochemical results show that the thinner the PPy coating, the higher rate the CF_x@PPy cathodes. CF_x@PPy cathode, with a PPy coating thickness of about 80 nm, delivers the highest power density of 7091 W kg^{-1} and the energy density of 565 Wh kg^{-1}. The EIS results indicate that the conductivity of CF_x@PPy can be improved by PPy coatings. Comparing with the discharged cathode of CF_x and CF_x@PPy cathode, it is found that the adsorptivity of CF_x has been improved by PPy coating. This favors the electrolyte infiltrating into the CF_x@PPy cathode. The PPy coating serves as the path for charges transfer, facilitating the successive lithium ions transfer between CF_x particles. However, too thick PPy coating may inhibit the lithium ions transfer and even pull down the discharge capacity.

References

1. J. Lee, A. Urban, X. Li, D. Su, G. Hautier, G. Ceder, *Science*, 343 (2014) 519.
2. K. Chen, D. Xue, *J. Mater. Chem. A*, (2016).
3. J. Liu, H. Xia, D. Xue, L. Lu, *J. Am. Chem. Soc.*, 131 (2009) 12086.
4. T. Nakajima, *J. Fluorine Chem.*, 149 (2013) 104.
5. M.A. Reddy, B. Breitung, M. Fichtner, *ACS Appl. Mater. Inter.*, 5 (2013) 11207.
6. J.C. Lu, Z.C. Liu, P. Huang, Q. Fang, M.H. Zhu, *Adv. Mater. Res.*, 704 (2013) 98.
7. G. Nagasubramanian, *Int. J. Electrochem. Sci.*, 2 (2007) 913.
8. P.J. Sideris, R. Yew, I. Nieves, K. Chen, G. Jain, C.L. Schmidt, S.G. Greenbaum, *J. Power Sources*, 254 (2014) 293.
9. E.Z. Kurmaev, A. Moewes, D.L. Ederer, H. Ishii, K. Seki, M. Yanagihara, F. Okino, H. Touhara, *Phys. Lett. A*, 288 (2001) 340.
10. H. Touhara, H. Fujimoto, N. Watanabe, *Solid State Ionics*, 14 (1984) 163.
11. J. Giraudet, C. Delabarre, K. Guérin, M. Dubois, F. Masin, A. Hamwi, *J. Power Sources*, 158 (2006) 1365.
12. H. Touhara, F. Okino, *Carbon*, 38 (2000) 241.
13. H. Touhara, K. Kadono, Y. Fujii, N. Watanabe, *Z. anorg. allg. Chem*, 544 (1987) 7.
14. C. Delabarre, M. Dubois, J. Giraudet, K. Guérin, A. Hamwi, *Carbon*, 44 (2006) 2543.
15. P.F. Fulvio, S.S. Brown, J. Adcock, R.T. Mayes, B. Guo, X.-G. Sun, S.M. Mahurin, G.M. Veith, S. Dai, *Chem. Mater.*, 23 (2011) 4420.
16. K. Matsumoto, J. Li, Y. Ohzawa, T. Nakajima, Z. Mazej, B. Žemva, *J. Fluorine Chem*, 127 (2006) 1383.

17. P. Hany, R. Yazami, A. Hamwi, *J. Power Sources*, 68 (1997) 708.
18. S.S. Zhang, D. Foster, J. Read, *J. Power Sources*, 188 (2009) 601.
19. S.S. Zhang, D. Foster, J. Read, *J. Power Sources*, 191 (2009) 648.
20. K. Guérin, R. Yazami, A. Hamwi, Electrochem. *Solid-State Lett*., 7 (2004) A159.
21. Y. Li, W. Feng, *J. Power Sources*, 274 (2015) 1292.
22. W. Yang, Y. Dai, S. Cai, Y. Zheng, W. Wen, K. Wang, Y. Feng, J. Xie, *J. Power Sources*, 255 (2014) 37.
23. A. Bahloul, B. Nessark, E. Briot, H. Groult, A. Mauger, K. Zaghib, C.M. Julien, *J. Power Sources*, 240 (2013) 267.
24. G.C. Li, G.R. Li, S.H. Ye, X.P. Gao, *Adv. Energy Mater.*, 2 (2012) 1238.
25. Q. Zhang, S. D'Astorg, P. Xiao, X. Zhang, L. Lu, *J. Power Sources*, 195 (2010) 2914.
26. L. Zhu, Y. Pan, L. Li, J. Zhou, W.X. Lei, J.H. Deng, Z.S. Ma, *Int. J. Electrochem. Sci.*, 11 (2016) 14.
27. H. Groult, C.M. Julien, A. Bahloul, S. Leclerc, E. Briot, A. Mauger, *Electrochem. Commun.*, 13 (2011) 1074.
28. Z.J. Zhang, J.Z. Wang, S.L. Chou, H.K. Liu, K. Ozawa, H.J. Li, *Electrochim. Acta*, 108 (2013) 820.
29. J. Cao, G. Hu, Z. Peng, K. Du, Y. Cao, *J. Power Sources*, 281 (2015) 49.
30. P. Lam, R. Yazami, *J. Power Sources*, 153 (2006) 354.
31. R. Yazami, A. Hamwi, K. Guérin, Y. Ozawa, M. Dubois, J. Giraudet, F. Masin, *Electrochem. Commun.*, 9 (2007) 1850.